Planar 0.05–1.1 THz Laminate-Based Transition Designs for Integrating High-Frequency Photodiodes With Rectangular Waveguides

Besher Khani ⬛, Sumer Makhlouf, Andreas G. Steffan, *Member, IEEE*, Jörg Honecker, and Andreas Stöhr, *Senior Member, IEEE*

Abstract—Compact planar laminate-based transitions for integrating high-frequency photodiodes (PDs) with rectangular waveguides (WRs) are presented for the WR15 to WR1 standard waveguide bands, i.e., from 0.05 THz up to 1.1 THz. The transitions couple the optically generated (e.g., via heterodyning) millimeter-wave or terahertz signals from the grounded coplanar waveguide (GCPW) output of the PD chip to the WR. To our knowledge, this is the first scalable integration concept that enables hermetic photodiode packaging up to the terahertz frequency range. For the WR15-WR6 bands, all transitions are designed on ultrathin microfiber reinforced PTFE composites (127-μm Rogers RT/duroid 5880 laminate). For the WR5-WR2.2 and the WR1.5-WR1 bands, liquid crystalline polymer ULTRALAM 3850 laminates are used with a thickness of 50 and 25 μm, respectively. The proposed GCPW-WR transition design is based on a double-slot antenna structure and enables the development of fully hermetic photonic packages, which is required to improve the durability of the PD chip. The transition designs are optimized by systematic EM-wave propagation modeling for achieving a wide operational bandwidth of up to 30% of the respective center frequency for each WR band. The optimized transitions exhibit an average insertion loss of about 1.5 dB and a return loss of about 10 dB for all waveguide bands (WR15-WR1). Based upon the systematic numerical modeling, generic guidelines are developed that allow designing a specific transition for any given waveguide band to 1.1 THz. In addition to the numerical analysis, GCPW-WR12 transitions for E-band (60–90 GHz) operation are fabricated and integrated with InP-based balanced-PD chips and GaAs HEMT MMIC medium power amplifiers in a fully hermetic package. Furthermore, hermetic WR12 coherent photonic mixer (CPX) modules are developed. The packaged WR12-type CPX allows direct optical-to-wireless conversion of optical baseband or IF-band signals, e.g., for radio-over-fiber fronthauling in mobile communications. The WR12-CPX module provides RF output power of up to +15 dB·m at 77.5 GHz.

Index Terms—Integrated optoelectronics, microwave photonics, photodetectors, slot antennas, terahertz radiation.

B. Khani, S. Makhlouf, and A. Stöhr are with the Institute of Optoelectronics, University of Duisburg-Essen, Duisburg 47057, Germany (e-mail: besher.khani@uni-due.de; sumer.makhlouf@uni-due.de; andreas.stoehr@uni-due.de).

A. G. Steffan and J. Honecker are with Finisar, Berlin 10553, Germany (e-mail: andreas.steffan@finisar.com; joerg.honecker@finisar.com).

I. INTRODUCTION

MANY bandwidth-hungry applications such as ultra-high-definition video streaming, new cloud-based services, or internet of things (IoT) were enabled by photonic network technologies. This is due to the huge available operational bandwidth offered by fiber-optic communications. In parallel, the ever-increasing demands for high data rate applications such as video streaming while being mobile are also pushing mobile communications, especially with respect to maximum cell capacity and latency. This has led to wireless communication systems which exploit carrier frequencies in the mm-wave and terahertz frequency ranges [1], where sufficient wide spectra are available to support these bandwidth-hungry applications. Consequently, mobile data traffic is expected to increase by twelve times from 2016 to 2022 [2].

By merging fiber-optic and radio-wave communication technologies, new converged fiber-wireless systems have been developed with exploit radio-over-fiber (RoF) antenna fronthaul and backhaul links. Already today, RoF supported terahertz communications has been demonstrated to support 59 Gbit/s per channel [3] and the 7 GHz slot allocated at the 60 GHz band can easily support 10 Gbit/s fiber-wireless RoF links [4]. Also, the E-band frequency slots at 71–76 GHz and 81–86 GHz are heavily used for medium and long range RoF wireless backhaul links [5]. In addition to communications, high-carrier frequencies are also required in several other applications, such as terahertz spectroscopy or medical-imaging applications [6], [7].

Among the available electronic and photonic technologies, high-frequency photodiodes (PDs) and optical heterodyning are widely used for converting optical baseband and IF band signals to mm-wave and THz radio frequency signals, as they offer comparably wide operational bandwidths [8]–[16]. For developing such mm-wave and THz-band photodiode modules, the optically generated mm-wave and THz signals can either be collimated in a quasi-optic approach using e.g., high-resistive Silicon lenses [9], [10] or the PD chip is integrated with a rectangular waveguide (WR) using a coplanar-to-WR transition [11]–[16]. Especially, the development of photodiode modules featuring a WR output is of great interest, since they are more convenient to integrate in systems than the quasi-optic PD modules. This is because the WR represents practically the only cost-efficient and low-loss approach to interconnect mm-wave

and THz PDs with other RF components such as amplifiers and antennas.

Here, in order to couple the optically generated mm-wave and THz signals from the PD chip to the WR output, a proper integration of the chip in a low-loss RF package is essential for decreasing the coupling losses. Many high-frequency PD modules with WR outputs, e.g., in the W-band (75–110 GHz) [13], in the F-band (90–140 GHz) [14], in the J-band (220–325 GHz) [15], and in the 400 GHz to 900 GHz frequency band [16] have been reported. Most of the reported mm-wave and THz photodiode modules either utilize E-field monopole antennas or dipole or parabolic antennas for end-fire coupling into the WR in a split-block package. In both cases, the PD packages are non-hermetic, i.e., the PD chip always faces atmosphere, which decreases the life time of the integrated PD chips. In addition, these packaging approaches suffer from complexity, bulky dimensions, and heavy weight [17].

In this work, we report on a compact planar laminate-based RF transition to interface the grounded coplanar waveguide output (GCPW) of high-frequency PD chips to a rectangular waveguide (WR). The presented GCPW-WR transition design is based on a double-slot antenna structure and enables the development of fully-hermetic and cost-efficient mm-wave and THz photodiode modules featuring a WR output. The manuscript is structured as follows: in Chapter II, we present the packaging concept for fully-hermetic photodiode modules utilizing planar GCPW-WR laminate-based transitions. In Chapter III, generic design guidelines are derived from systematic electromagnetic-field full-wave simulations. These guidelines allow designing a transition for any given waveguide band between 50 GHz and 1.1 THz (WR15-WR1) using commercially available ultra-thin laminates. Chapter IV reports on the fabrication of a GCPW-WR12 transition and the integration and packaging of an InP-based high-frequency balanced photodiode (BPD) chip and a GaAs HEMT MMIC medium power amplifier. The fabricated hermetic module provides an RF output power up to +15 dBm at 77.5 GHz. According to authors' knowledge, this is the highest reported output power level radiated directly from a photodiode module in that frequency range.

II. COHERENT PHOTOMIXING FOR RF SIGNALS GENERATION

Fig. 1 illustrates the proposed module which is designed for converting an optical baseband or IF band signal to mm-wave or THz signal by optical heterodyning. In order to distinguish the specific function of the presented device from a coherent optical receiver that basically converts optical baseband to electrical baseband in 100 Gbit/s or 400 Gbit/s fiber-optic communications, the device is named coherent photonic mixer or coherent photomixer (CPX).

The concept for developing a hermetic CPX module is shown in Fig. 2. Basically, the idea is to use the planar GCPW-WR transition not only to couple the EM-wave from the PD chip to the WR but also to seal the package by placing the transition on top of the WR flange as shown in Fig. 2. This way, the transition completely covers the WR aperture, which isolates the PD chips from humidity and dust. The vias are fully surrounding
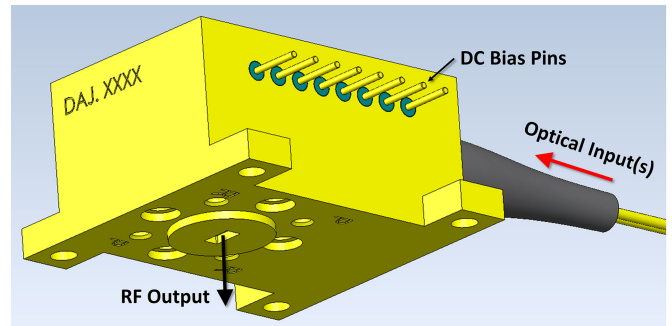

Fig. 1. Proposed package design of the fully-hermetic photodiode module featuring a rectangular waveguide output and optical input(s) feeding the photodiode (PD) chip.
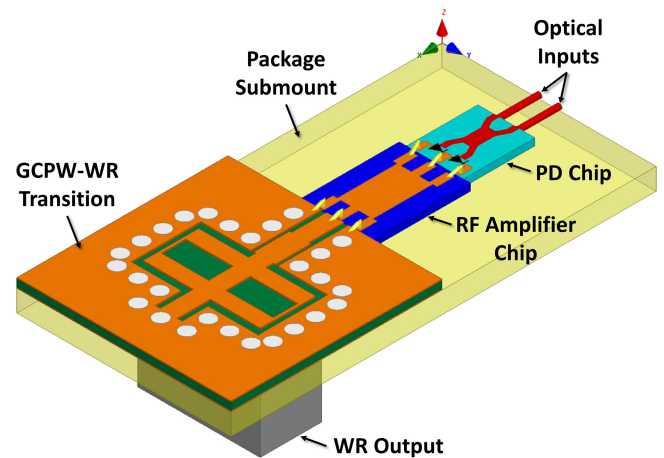

Fig. 2. Integration concept of the fully-hermetic photodiode module using a planar grounded coplanar waveguide to rectangular waveguide (GCPW-WR) transition, an RF amplifier chip, and a balanced photodiode (BPD) chip for coherent photomixing and optical-to-wireless conversion.

the transition, i.e., they are outside the WR aperture and are not facing atmosphere.

Furthermore, in this work, we consider the integration of balanced photodiode (BPD) chips rather than single photomixers. The reason is that the use of a balanced photomixer results in a theoretically 6 dB higher RF output power compared to a single photomixer [18]. This is simply because by using a monolithically integrated 3-dB coupler and a BPD, the total optical power of the signal and LO lasers can be utilized for optical-to-RF conversion. In case of a single photomixer, only half the total optical input power would be used resulting in a 6 dB RF loss. The GCPW-WR transition, illustrated in Fig. 2, is based on a double-slot antenna which radiates the optically generated RF signal through the laminate into the rectangular waveguide. This seals the package as described above and also eliminates the need for the bulky and expensive split-block technology.

The BPD chip can be bonded to the transition laminate either by wire, ribbon, or flip-chip bonding. The utilized bonding method depends on the operating frequency of the module. For frequencies above 100 GHz, wire bonds behave as a distributed component and become lossy [17]. Here, ribbon or flip-chip
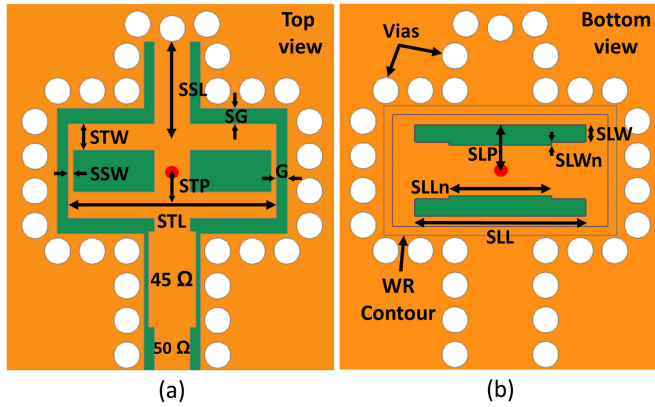
Fig. 3. Design of the grounded coplanar waveguide to rectangular waveguide (GCPW-WR) transition: (a) top view, and (b) bottom view.
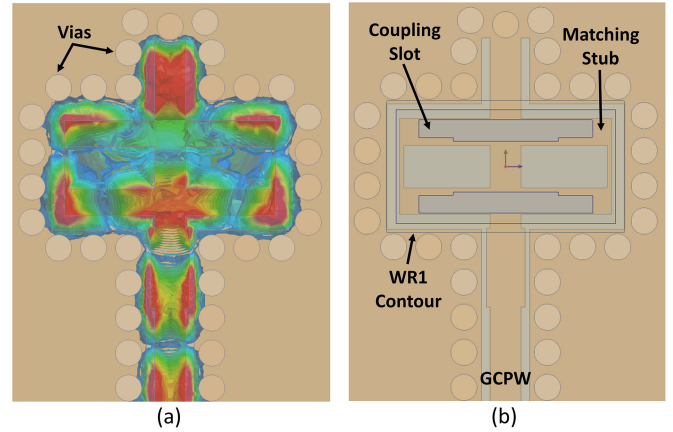

Fig. 4. GCPW-WR1 double-slot transition: (a) electric field distribution at 990 GHz, and (b) transparent view of the transition's laminate showing the slots on the ground in contrast to the matching stubs' position on the top metal. Via diameter is 30 μm, pitch distance is 40 μm.

bonds can be used instead for frequencies at least up to 500 GHz [15], [19].

In order to provide sufficient output power levels for enabling wireless communications over reasonable distances, the BPD chip is integrated with an RF amplifier to boost the output power. This is to eliminate the necessity to use external and bulky amplifiers.

III. TERAHERTZ GCPW-WR DOUBLE-SLOT TRANSITIONS

First, the transition consists of double-slots etched at the backside of the laminate, as shown in Fig. 3(b). The RF signal is coupled out into the rectangular waveguide directly through the double-slots that are facing the WR input. Here, the use of the double-slot structure on the ground-side of the laminate, increases the coupling bandwidth and overcomes the poor return loss problem caused by using a single-slot structure [20]. Second, the transition consists of two matching- stubs placed on top of the slots, as shown in Fig. 3(a). The accurate placing of the matching stubs over the coupling-slots decreases the radiation loss and improves the coupling efficiency from the coplanar to the rectangular waveguide. The matching-stubs' position, in contrast to the coupling-slots and the WR contour, is shown in Fig. 4(b). Third, metalized vias surround the transition structure to prevent surface mode propagation. Since the transition laminate is mounted directly on top of the WR, it completely covers the aperture and thus isolates the internal components of the photodiode module. This allows the development of a fully-hermetic modules.

A. Operating Principle and Design Parameters

The symmetry of the double-slot structure assures the power splitting equality between both stubs, thus resulting in equal fields' distribution in both directions: the GCPW input port and the short-circuited stub port. The waves propagating toward the center of the stubs are out of phase canceling each other [21]. Therefore, there is no E-field observed at the center, as shown from the E-field distribution of the GCPW-WR1 transition at 990 GHz, Fig. 4(a). The short-circuited stub length (*SSL*) is equal to half effective wavelength, resulting in an in-phase

TABLE I
DESIGN PARAMETERS OF THE GCPW-WR DOUBLE-SLOT TRANSITION

Parameter	Value	Description
SLL	$\lambda_0 / 2$	slot length
SLW	$15.6\% \cdot b$	slot width
SLP	$41\% \cdot b$	slot position
SLLn	$0.61 \cdot SLL$	slot notch length
SLWn	$0.2 \cdot SLW$	slot notch width
STL	λ_{eff}	stub length
STW	$24\% \cdot b$	stub width
STP	$31\% \cdot b$	stub position
SSW	$G / 2$	stub short width
SSL	$\lambda_{eff} / 2$	stub short length
SG	$1.5 \cdot G$	stub gap

G: width of the GCPW gap, *b*: height of the rectangular waveguide.

accumulation of the waves at the stubs. The advantage of the short-, compared to the open-circuited stub, is that it is less prone to leakage of electromagnetic radiation and is easier to realize. The matching stub length (*STL*) is equal to one effective wavelength of the center frequency and the length of each coupling-slot (*SLL*) is half wavelength at the lower band frequency. The circuit model of the reported GCPW-WR transition and the waves flow are presented in [21]. The transition has been further optimized by adding: (1) a shorter notch to the coupling slots toward the center of the rectangular waveguide, and (2) a capacitive 45 Ω GCPW line before the antenna structure in order to achieve better matching [22]. The notch geometry and the transition design guidelines are summarized in Table I. The design parameters are mainly function to the effective wavelength (λ_{eff}) and the rectangular waveguide height (*b*). They are also valid for designing the transition on any high-frequency laminate at any waveguide standard. Next, the designed transitions are numerically analyzed using a full-wave 3D electromagnetic field simulation software based on the finite element method (ANSYS HFSS). The transitions were designed on two different ultra-thin high-frequency laminates for waveguide standards from WR15 to WR1. The design parameters have been derived and optimized based on the EM-wave numerical analysis.

TABLE II
GCPW-WR DOUBLE-SLOT TRANSITION DESIGN FROM 50 GHz UP TO 1.1 THz

| Waveguide Standard	Frequency Range	1-dB BW	Laminate Thickness (h)	h/λ_{eff}	ε_e	50 Ω GCPW G-S-G, μm	Max. Group Delay	Min. IL	Max. RL
WR15	50-68 GHz	30%	127 μm	3.8%	1.76	100-320-100	90 ps	2 dB	10 dB
WR12	67-90 GHz	29%	127 μm	5%	1.77	100-320-100	60 ps	1.4 dB	10 dB
WR8	90-122 GHz	30%	127 μm	7%	1.82	100-320-100	55 ps	1.1 dB	9 dB
WR6	122-160 GHz	27%	127 μm	9%	1.7	50-250-50	50 ps	1 dB	8 dB
WR5	160-217 GHz	30%	50 μm	5.5%	2.22	35-120-35	35 ps	1.7 dB	10 dB
WR3	217-291 GHz	29%	50 μm	7.3%	2.29	35-120-35	26 ps	1.6 dB	8 dB
WR2.8	291-389 GHz	29%	50 μm	9.9%	2.35	30-100-30	18 ps	1.2 dB	11 dB
WR2.2	389-500 GHz	25%	50 μm	12.5%	2.18	25-85-25	13 ps	1.3 dB	8 dB
WR1.5	500-676 GHz	30%	25 μm	9%	2.2	15-48-15	12 ps	1.7 dB	10 dB
WR1.2	676-880 GHz	26%	25 μm	10.5%	2.1	12-41-12	9 ps	1.3 dB	11 dB
WR1	0.88-1.1 THz	22%	25 μm	13.4%	2.16	10-35-10	6 ps	1.3 dB	8 dB
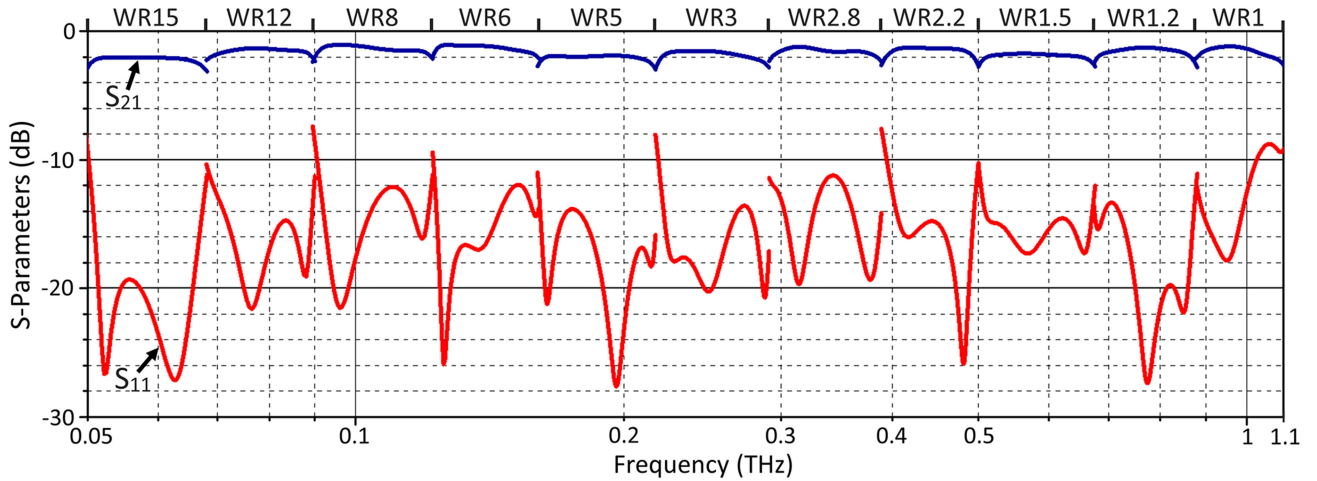
Fig. 5.   Numerical analysis of the GCPW-WR double-slot transition up to 1.1 THz (WR15-WR1).

B. Numerical Analysis up to 1.1 THz

For designing high-frequency and wideband mm-wave and THz circuitries, several considerations have to be taken into account. First and the most important factor, for high data-rate applications, is the transmission line (TL) dispersion, which results in increased bit error rates [23]. Dispersion occurs in non-homogeneous TLs, like GCPW or microstrip, resulting in a non-linear propagation constant. In this case, the energy will propagate at different group velocities as the frequency changes, thus causing different arrival times for the energies at different frequencies. Therefore, the deviation of the phase constant as a function of the radiating frequency (group delay) has to be minimized. In this matter, the proper choice of the substrate thickness (h) will affect the dispersion. The thicker the substrate is, the more inhomogeneous the TL will be, which results in a more dispersive line. Hence, the ratio of the laminate thickness to the effective wavelength (h/λ_{eff}) has to be minimized in order to guarantee smaller dispersion values. Therefore, ultra-thin laminates are used to design mm-wave and THz GCPW-WR transitions. In addition, choosing low-dielectric laminates is important for maintaining low dispersion values. For a given laminate thickness (h), the lower the dielectric constant (ε_r) is, the more homogenous the transmission line will be, resulting in a reduced (h/λ_{eff}) value. For a

successful design, it is important to maintain this ration below 15% [23].

Based on the previous discussions, we have chosen the Rogers RT/duroid 5880 laminate ($\varepsilon_r = 2.2$, $h = 127\,\mu$m, tan $\delta = 0.0009$) for designing the WR15-WR6 waveguide transitions and the Rogers ULTRALAM 3850 laminate ($\varepsilon_r = 2.9$, tan $\delta = 0.0025$) with $h = 50\,\mu$m for WR5-WR2.2 and $h = 25\,\mu$m for WR1.5-WR1 waveguides. Both laminates have low moisture absorption [24] (0.02% for Rogers 5880 and 0.04% for Rogers 3850). The dielectric loss tangents of the substrates are included in the simulations. In addition, the metal conductivity of 5.8×10^7 S/m is also considered. The S-parameters simulations are carried out under driven modal solution type and both the GCPW port and the WG port are wave ports and operate under the dominant mode. Table II summarizes the main design parameters and RF performances of the WR15-WR1 grounded coplanar waveguide to rectangular waveguide transitions together with their corresponding RF laminates. In addition, the operating frequency ranges of the transitions together with their 1-dB coupling bandwidths are also presented in Table II, as well as, the dimensions of the 50 Ω GCPWs, the effective dielectric constants (ε_e), and the calculated h/λ_{eff} ratios, for each RF laminate. Finally, Fig. 5 concludes the numerical S-parameters (IL: S_{21} and RL: S_{11}) of the designed GCPW-WR double-slot
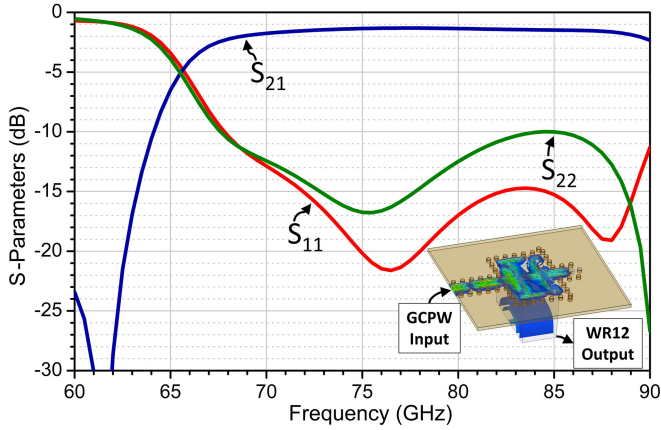
Fig. 6. Numerical S-parameters of the designed GCPW-WR12 double-slot transition. The inset shows the magnitude of the electric field distribution at 80 GHz.
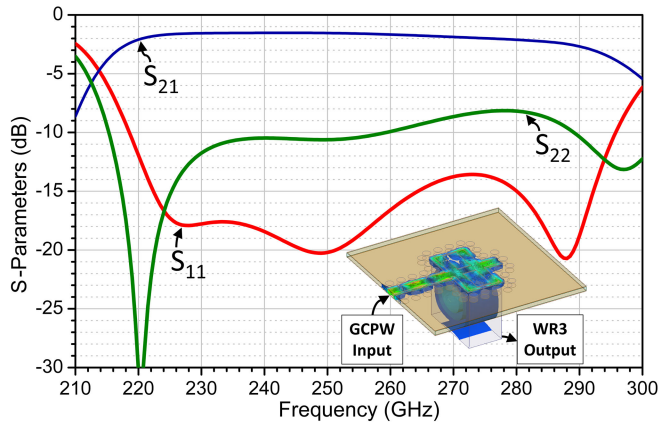

Fig. 7. Numerical S-parameters of the designed GCPW-WR3 double-slot transition. The inset shows the magnitude of the electric field distribution at 277 GHz.

transitions for waveguide standards from WR15 to WR1, covering both the mm-wave and terahertz frequencies up to 1.1 THz. An insertion loss (IL) in a range of about 1.5 dB and a return loss (RL) of about 10 dB have been achieved for all waveguide bands. A list of minimum IL, maximum RL, and maximum group delay values are listed in Table II. A coupling bandwidth up to 30% of the respective center frequency of each waveguide band has been achieved. This outperforms the coupling bandwidth of the double-slot transitions presented in [25] and [26] by up to 8%.

Figs. 6 and 7 show the extended numerical S-parameters of the designed WR12 and WR3 transitions, respectively, including the return loss at the rectangular waveguide port (S_{22}). Here, the bandwidth of the designed WR12 transition outperforms the one presented in [22]. Thus, allowing not only to cover the 70 GHz slot (71–76 GHz) of the E-band frequency range, however also the 80 GHz one (81–86 GHz).

IV. PACKAGED COHERENT PHOTONIC MIXERS (WR12-CPXS)

Based on the presented systematic modeling and design guidelines, an optimized E-band (70/80 GHz) GCPW-WR12
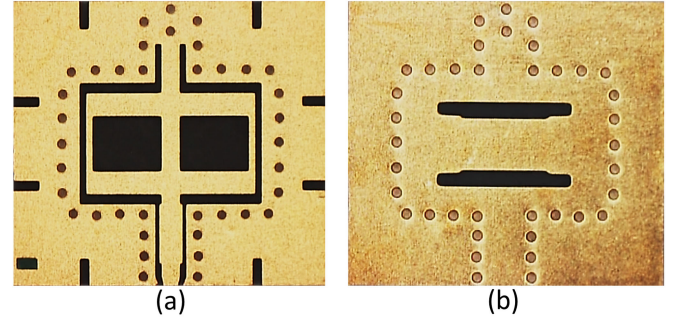

Fig. 8. (a) Top view, (b) bottom view of the fabricated GCPW-WR12 E-band (70/80 GHz) double-slot transition based on ROGERS RT/duroid 5880 laminate.

double-slot transition has been fabricated on a 127 μm RO5880 laminate. A top and bottom view of the fabricated WR12 transition are shown in Figs. 8(a) and (b), respectively. The size of the fabricated WR12 transition is 4.8 $\times$ 5.5 mm^2 and it has eight alignment markers etched at the edges of the laminate to precisely position the slots on top of the WR12 input. The transition laminate is glued on top of the WR aperture using silver-filled epoxy (H20E) and it completely covers the WR. By integrating the fabricated transition with a balanced PD chip via wire bonding, an E-band fully-hermetic coherent photonic mixer (WR12-CPX) featuring a rectangular waveguide output has been developed, as shown in Fig. 9. Unlike the transitions based on wire-probe coupling [27] or ridge-waveguide discontinuities [28], here the presented double-slot transition neither requires a probe-fed configuration nor a specially machined waveguide. The developed WR12-CPX also comprises two pigtailed optical fiber inputs. The first input is either fed by an optical data signal for upconversion or by an unmodulated optical signal for RF signal generation. The other input is fed by an optical local oscillator (LO) signal generated by a tunable free-running laser-diode (LD). In this aspect, the use of laser-diodes operating at 1.55 μm telecom wavelength standard has an advantage in developing affordable THz systems and components. The fabricated BPD chip is InP-based and consists of a 2 $\times$ 2 multi-mode interferometer (MMI) monolithically integrated with two *pin*-type waveguide photodiodes in a balanced configuration. It also features an on-chip DC-bias circuitry for each PD. The 2 $\times$ 2 MMI guarantees the symmetrical optical injection into the PD pair.

In contrast to the V-type CPX presented in [18], here the WR12-CPX enables direct optical-to-wireless conversion without the need to use any external bulky coaxial-to-WR adapter. The presented module is also provided with DC pins for external biasing of the BPD chip. The package design allows to accommodate the screws and pins of the standard WR flange. Fig. 10 shows a microphotograph of the internal structure of the WR12-CPX. In addition, for enabling a long-distance RoF wireless links, the transition is also integrated with a commercial off-the-shelf GaAs HEMT MMIC medium power amplifier (MPA) and a BPD chip for developing a high-power coherent photonic mixer. The MPA chip (HMC-AUH320) operates
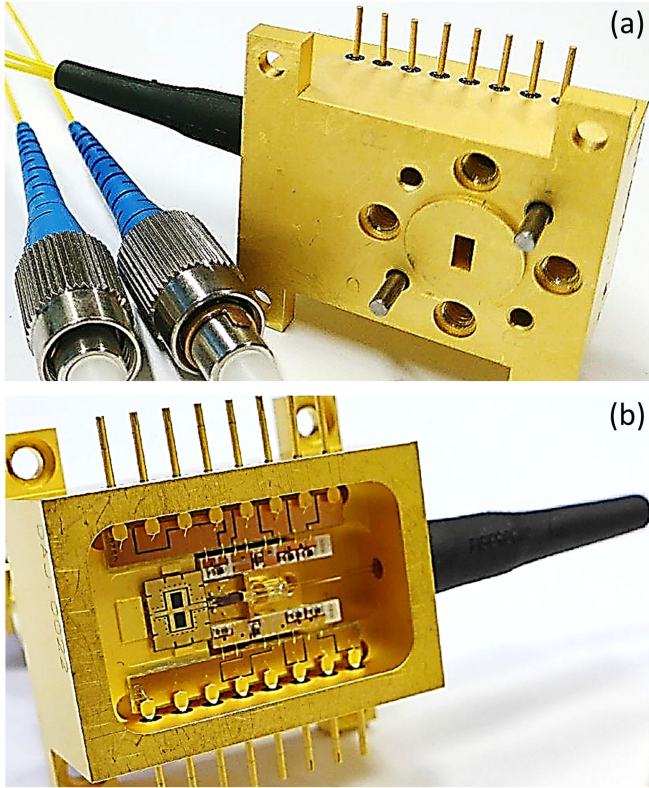
Fig. 9.   Photograph of the packaged E-band coherent photonic mixer (WR12-CPX) for direct optical-to-wireless conversion: (a) bottom view showing the WR12 output and the two optical inputs, (b) top internal view showing the transition laminate, the balanced photodiode (BPD) chip, the fiber to chip coupling, and the DC circuitries.
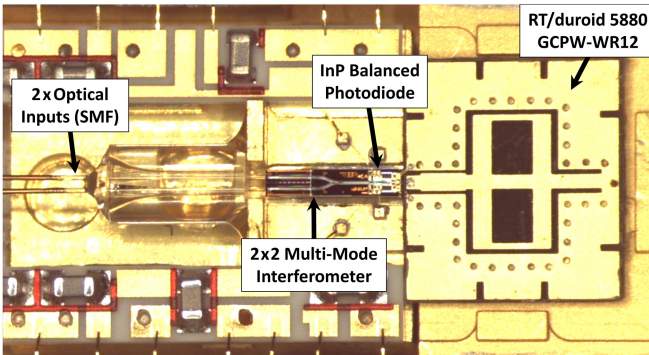

Fig. 10.   Microphotograph of the E-band (70/80 GHz) WR12-CPX in hermetic package showing the fiber-to-chip coupling, the BPD chip, and the transition laminate.

between 71 GHz and 86 GHz and it has a maximum gain of 16 dB at 74 GHz with a 1-dB compression at +15 dBm. It requires +4 V of supply voltage and its CPW input/output are matched to a 50 Ohm load. The size of the MPA chip is 2.2 × 0.87 × 0.1 mm^3. Fig. 13 shows a microphotograph of the internal structure of the high-power WR12-CPX. Furthermore, the hermeticity has been tested by measuring the helium leakage rate through the fabricated transitions. The measured leakage rate after Helium exposure was 3×10^{-7} mbar. *l/s*. This means that the transition is tight against atmospheric gas leakage.
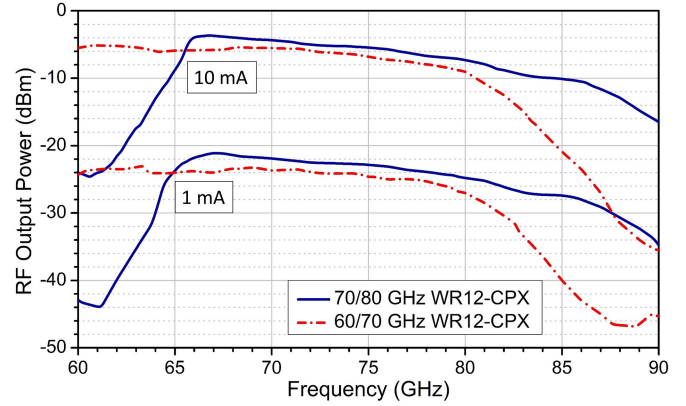

Fig. 11.   RF responsivity measurements of the optimized E-band 70/80 GHz and 60/70 GHz WR12-CPX at a photocurrent of 10 mA and 1mA.
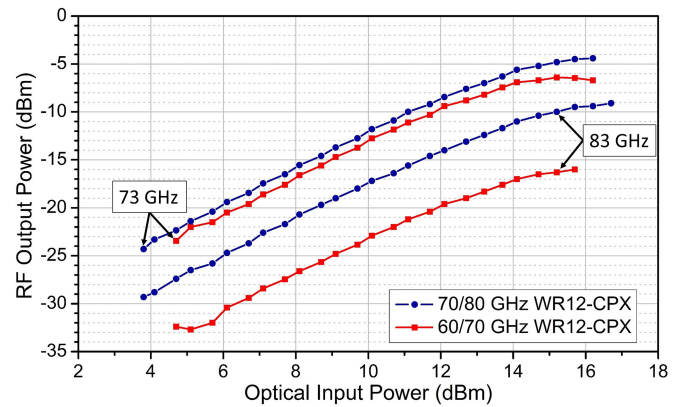

Fig. 12.   Measured RF output power versus the total optical signal power fed into the 70/80 GHz and 60/70 GHz WR12-CPXs at 73 GHz and 83 GHz.

A. RF Responsivity of the Integrated WR12-CPX

The packaged WR12-CPXs have been experimentally characterized using two free-running laser diodes (LDs) and an RF power meter at the WR12 output. By fixing the optical signal of the first LD and tuning the second one within the optical C-band, the E-band signal (60–90 GHz) is generated and coupled out from the WR12 output. The RF responsivity of the packaged 70/80 GHz WR12-CPX is then measured at photocurrent values of 10 mA and 1 mA, as shown in Fig. 11. Its responsivity is further compared to the 60/70 GHz WR12-CPX module that was presented in [29], which was based on the 60/70 GHz GCPW-WR12 transition design reported in [30]. Overall, the generated RF output power from the optimized 70/80 GHz module is higher than that of the 60/70 GHz one, reaching a difference up to +14 dB at 86 GHz. Thus, the presented 70/80 GHz design is best optimized to cover both E-band slots (71–76 GHz and 81–86 GHz), succeeding RF output power levels up to −5 dBm and −9 dBm at 73 GHz and 83 GHz, respectively, without RF amplification. Fig. 14 shows the RF responsivity of the high-power WR12-CPX achieving RF output power levels up to +15 dBm at 77.5 GHz. It is also compared to the RF responsivity of the 70/80 GHz module without amplification that was presented in Fig. 10. The responsivity of the WR12-CPX is 0.4 A/W.
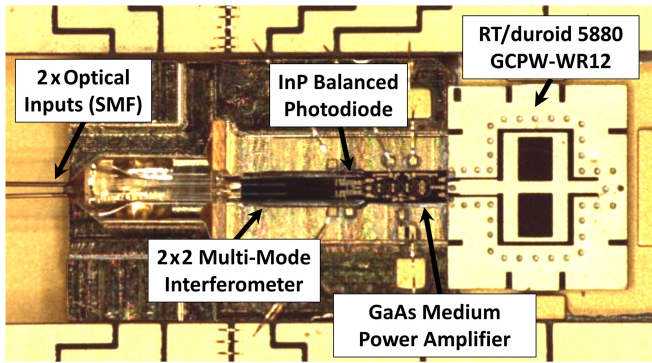
Fig. 13. Microphotograph of high-power E-band 70/80 GHz WR12-CPX in hermetic package showing the fiber-to-chip coupling, the BPD chip, the amplifier chip, and the transition laminate.
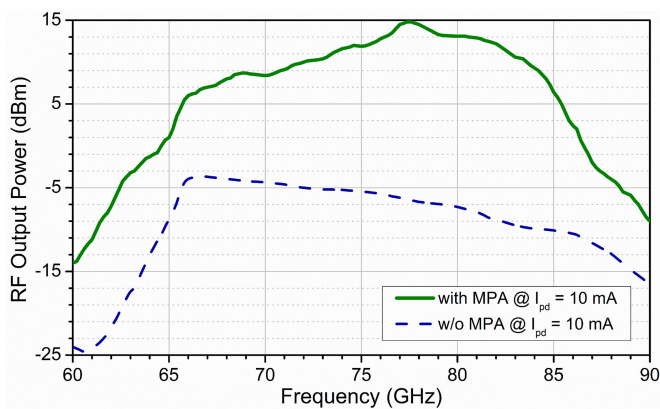

Fig. 14. RF responsivity measurements of the E-band 70/80 GHz WR12-CPX with and without amplifier (MPA) integration.
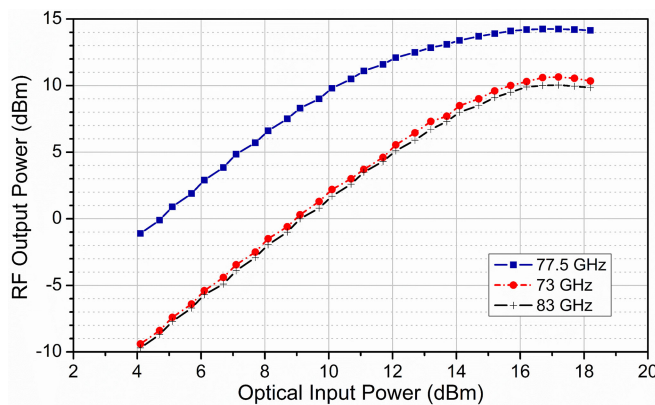

Fig. 15. Measured RF output power versus the total optical signal power fed into the high-power 70/80 GHz WR12-CPX.

B. 1-dB Saturation Power Measurement

The RF output power is also measured versus the total optical signal power fed into the WR12-CPX module. Fig. 12 compares the RF output power levels at 73 GHz and 83 GHz for both the 70/80 GHz and 60/70 GHz modules. The 70/80 GHz module outperforms the 60/70 GHz one by at least 1 dB at

73 GHz and 6 dB at 83 GHz. By increasing the optical input power levels above +12 dBm, saturation behavior has been observed. Hence, limiting the maximum RF output power of the 70/80 GHz WR12-CPX to −4 dBm. The 1-dB saturation point for this device was measured to be +13 dBm. The optical input powers that corresponds to 1 mA and 10 mA of photocurrents are +5 dBm and +14.5 dBm, respectively. The RF output power versus the optical input power for the high-power WR12-CPX is also measured at 73 GHz, 77.5 GHz, and 83 GHz, as shown in Fig. 15. The maximum measured RF power is about +15 dBm at 77.5 GHz. According to authors' knowledge, this is the highest reported output power level radiated directly form a photodiode module in the E-band frequency range.

V. Conclusion

This manuscript developed generic rules for designing planar laminate-based transitions for interconnecting the 50 Ω grounded coplanar waveguide outputs of high-frequency photodiode chips to rectangular waveguides (WRs) within the frequency range between 50 GHz to 1.1 THz. To our knowledge, this is the first scalable transition concept that enables hermetic photodiode packaging up to the terahertz frequency range.

All transitions feature a double-slot antenna structure and are based upon ultrathin ROGERS laminates. Each transition is optimized for supporting an operational bandwidth of about 30% of the respective WR center frequency. The average insertion loss and return loss for all transitions are 1.5 dB and 10 dB, respectively.

For the E-band (60–90 GHz) operation, GCPW-WR12 transitions were fabricated on Rogers 5880 laminate and integrated with balanced waveguide photomixer chips and medium-power amplifiers. The integrated chips and transitions were hermetically packaged in a Kovar module, which sealed by a metallic lid. The developed E-band coherent photomixer (CPX) module provides a maximum output RF power of +15 dBm.

Generally, it is shown that the presented transitions allow the integration of single and balanced photomixers and photodiodes within the frequency range from 0.05 THz up to 1.1 THz. However, since the transition design is generic and reciprocal, it could also be employed for packaging other photonic or electronic components and used for coupling EM-waves from the WR to a GCPW. Generally, this allows to use the transitions also for packaging high-frequency optical modulator or receiver antennas.

References

[1] T. Nagatsuma *et al.*, "Millimeter-wave and terahertz-wave applications enabled by photonics," *IEEE J. Quantum Electron.*, vol. 52, no. 1, Jan. 2016, Paper no. 0600912.

[2] Ericsson Mobility Report, Ericsson Mob. Rep., pp. 1–36, Jun. 2017.

[3] A. Stöhr *et al.*, "Coherent radio-over-fiber THz communication link for high data-rate 59 Gbit/s 64-QAM-OFDM and real-time HDTV transmission," in *Proc. Opt. Fiber Commun. Conf. Exhib.*, Los Angeles, CA, USA, 2017, Paper no. Tu3B.2.

[4] S. S. Dhillon *et al.*, "The 2017 terahertz science and technology roadmap," *J. Phys. D, Appl. Phys.*, vol. 50, 2017, Paper no. 043001.

[5] R. Chuenchom *et al.*, "Wireless extension for 2.5 Gbit/s GPON," in *Proc. Opt. Fiber Commun. Conf. Exhib.*, San Diego, CA, USA, 2018, Paper no. Th3G.2.

[6] H. Takeda *et al.*, "0.6–1.6 THz band spectroscopy of organic thermally activated delayed fluorescence materials," *Opt. Mater. Express*, vol. 6, no. 10, pp. 3045–3052, Oct. 2016.

[7] S. Hisatake, J.-Y. Kim, K. Ajito, and T. Nagatsuma, "Self-heterodyne spectrometer using uni-traveling-carrier photodiodes for terahertz-wave generators and optoelectronic mixers," *J. Lightw. Technol.*, vol. 32, no. 20, pp. 3683–3689, Oct. 2014.

[8] V. Rymanov *et al.*, "Triple transit region photodiodes (TTR-PDs) providing high millimeter wave output power," *Opt. Express*, vol. 22, no. 7, pp. 7550–7558, Apr. 2014.

[9] A. Rivera-Lavado *et al.*, "Dielectric rod waveguide antenna as THz emitter for photomixing devices," *IEEE Trans. Antennas Propag.*, vol. 63, no. 3, pp. 882–890, Mar. 2015.

[10] V. Rymanov *et al.*, "Lens-assisted quasi-optical THz transmitter employing antenna-integrated triple transit region photodiodes," in *Proc. Int. Top. Meeting Microw. Photon.*, Beijing, China, 2017, pp. 1–4.

[11] G. Zhou *et al.*, "High-power InP-based waveguide integrated modified uni-traveling-carrier photodiodes," *J. Lightw. Technol.*, vol. 35, no. 4, pp. 717–721, Feb. 2017.

[12] H. J. Song, K. Ajito, Y. Muramoto, A. Wakatsuki, T. Nagatsuma, and N. Kukutsu, "Uni-travelling-carrier photodiode module generating 300 GHz power greater than 1 mW," *IEEE Microw. Wireless Compon. Lett.*, vol. 22, no. 7, pp. 363–365, Jul. 2012.

[13] P. G. Huggard *et al.*, "Efficient generation of guided millimeter-wave power by photomixing," *IEEE Photon. Technol. Lett.*, vol. 14, no. 2, pp. 197–199, Feb. 2002.

[14] H. Ito, T. Ito, Y. Muramoto, T. Furuta, and T. Ishibashi, "Rectangular waveguide output uni-traveling-carrier photodiode module for high-power photonic millimeter-wave generation in the F-band," *J. Lightw. Technol.*, vol. 21, no. 12, pp. 3456–3462, Dec. 2003.

[15] H. Ito *et al.*, "Photonic millimetre- and sub-millimetre-wave generation using j-band rectangular-waveguide output uni-travelling-carrier photodiode module," *Electron. Lett.*, vol. 42, no. 24, pp. 1424–1425, Nov. 2006.

[16] T. Kurokawa *et al.*, "Over 300 GHz bandwidth UTC-PD module with 600 GHz band rectangular-waveguide output," *Electron. Lett.*, vol. 54, no. 11, pp. 705–706, May 2018.

[17] H.-J. Song, "Packages for terahertz electronics," *Proc. IEEE*, vol. 105, no. 6, pp. 1121–1138, Jun. 2017.

[18] R. Chuenchom *et al.*, "E-band 76-GHz coherent RoF backhaul link using an integrated photonic mixer," *J. Lightw. Technol.*, vol. 34, no. 20, pp. 4744–4750, Oct. 2016.

[19] S. Sinha *et al.*, "Flip-chip approach for 500 GHz broadband interconnects," *IEEE Trans. Microw. Theory Techn.*, vol. 65, no. 4, pp. 1215–1225, Apr. 2017.

[20] H. Aliakbarian *et al.*, "Novel low-cost end-wall microstrip-to-waveguide splitter transition," *Prog. Electromagn. Res.*, vol. 101, pp. 75–96, 2010.

[21] H. Aliakbarian *et al.*, "Analysis of the doubled-slot end-wall waveguide to CPW transition," in *Proc. Int. Symp. Antennas Propag.*, Spokane, WA, USA, 2011, pp. 1–4.

[22] I. Flammia *et al.*, "Novel E-band (71–76 GHz) photodiode module featuring a hermetic grounded-coplanar-waveguide-to-rectangular-waveguide transition," in *Proc. Int. Top. Meeting Microw. Photon.*, Singapore, 2011, pp. 405–408.

[23] K. Kuang *et al.*, *RF and Microwave Microelectronics Packaging*. New York, NY, USA: Springer, 2010.

[24] Rogers Corporation, publication no. 92–101 and 92–125, 2018. [Online]. Available: https://www.rogerscorp.com

[25] S. Radiom *et al.*, "A fully micromachined W-band waveguide-to-grounded coplanar waveguide transition for 91–113 GHz applications," in *Proc. Eur. Microw. Conf.*, Paris, France, 2010, pp. 668–670.

[26] H. Aliakbarian *et al.*, "A fully micromachined double-slot waveguide-To-GCPW transition for 180–230 GHz mm-wave applications," in *Proc. Int. Conf. Ultra-WideBand*, Paris, France, 2014, pp. 394–397.

[27] T. Q. Ho and Y. Shih, "Spectral-domain analysis of E-plane waveguide to microstrip transitions," *IEEE Trans. Microw. Theory Techn.*, vol. 37, no. 2, pp. 388–392, Feb. 1989.

[28] L. J. Lavedan, "Design of waveguide-to-microstrip transition specially suited to millimeter wave applications," *Electron. Lett.*, vol. 13, no. 20, pp. 604–605, Sep. 1977.

[29] B. Khani *et al.*, "Fully-packaged 71–76 GHz coherent photonic mixer featuring WR-12 output for CRoF backhauling," in *Proc. Eur. Conf. Opt. Commun.*, Düsseldorf, Germany, 2016, pp. 1–3.

[30] B. Khani *et al.*, "Compact rectangular-waveguide (WR-12) transition for coherent photonic mixers," in *Proc. Global Symp. Millim. Waves*, Espoo, Finland, 2016, pp. 1–3.

Besher Khani received the Master's degree (M.Sc.) in computer science and communications engineering from the University of Duisburg-Essen in 2013.

After his study, he has gained international experience working in the Department of Electronics Technology, Charles III University of Madrid within the Marie Curie "MITEPHO" (Microwave and TErahertz PHOtonics), focusing on the design of novel millimeter-wave circuits using the finite-element method high frequency structural simulator. Since 2014, he has been a member of the Optoelectronics Department, University of Duisburg-Essen. He has authored or coauthored more than 30 papers in refereed journals and conferences. His current research interests focus on the design and development of compact millimeter-wave and THz coherent photonic transmitters and receivers modules for the 5G mobile communications and photonic radar applications. His research includes III/V and RF photonic integration technologies based on high-frequency laminates.

Sumer Makhlouf received the Master's degree (M.Sc.) in communications engineering from the University of Duisburg-Essen in 2018, and is currently working toward the Ph.D. degree in THz interconnectors. His Master's thesis concentrated on the 3-D-printed THz photodiode packages with rectangular waveguide output. He is currently a member of the Optoelectronics Department within the Center for Semiconductor Technology and Optoelectronics (ZHO) and a Research Associate with the University of Duisburg-Essen.

Andreas G. Steffan (M'10) received the Dipl. Ing. and Dipl. Phys. degrees from the Rheinisch-Westfälisch Technische Hochschule Aachen, and the Ph.D. degree from the University of Cambridge, U.K., in 2002. For his thesis, he worked on silicon-on-insulator waveguides. This work was carried out at the Institute of Semiconductor Technology in cooperation with AMO GmbH, Aachen. In 2002, he joined u²t Photonics AG, now Finisar. Initially, he was a Project Manager on the development of new transmitter, receivers and test and measurement products, including modulators and pulsed laser sources. At Finisar, he is currently heading the T&M /Analogue Products Group.

Dr. Steffan is a Member of the Institute of Physics, and received awards from the Engineering and Physical Science Research Council, Renishaw plc., and the Cambridge European Trust.

Jörg Honecker received the Dipl. Ing. after studying four years of communication engineering with his main focus on high frequency technology, digital signal handling and transfer mode system. He has been with Finisar and before u²t Photonics AG as a Development Engineer since September 2000. During his study, he was also with Heinrich Hertz Institute on different projects, especially in the field of optical techniques. At FIN, he is in charge of RF simulation of our devices and all kinds of measurements of high frequencies up to 110 GHz. Since his Diploma, he has been continuously focusing on RF measurement techniques with the 67-GHz lightwave component analyzer which is similar to a network analyzer with optical interfaces. This makes him an expert in this very important field of measurement techniques.

Andreas Stöhr (SM'97) received the Dipl.-Ing. and Dr.-Ing. degrees in electrical engineering from Gerhard-Mercator-University, Germany, in 1991 and 1997, respectively.

From 1987 until 1996, he was the CEO of MS Steuerungsanlagen GmbH in Germany. From 1996 until 2013, he was a Research Scientist with the University Duisburg. During that period, in 1998 and 1999, he also joined the Communications Research Laboratory in Tokyo, Japan, where he worked on 60-GHz wireless systems employing radio over fiber techniques. He was also with France Telecom Orange Labs, Lannion, France, in 2009, and with Corning in 2015. He is currently also a Visiting Professor with the University of Ottawa. Since 2011, he has been a Professor and the Head of the Optoelectronics Department within the Center for Semiconductor Technology and Optoelectronics (ZHO), University Duisburg-Essen, Germany. He has authored or coauthored more than 200 papers in refereed journals and conferences. His current research interests include III/V integrated microwave photonic device technology and RF photonic integration technologies for millimeter-wave and THz communications, measurement systems as well as sensing applications.

Dr. Stöhr is a Senior Member of IEEE Photonics and MTT societies, Committee Member and Chair of a number of international conferences and IEEE/OSA guest editor.